Mineralogy and Petrology
https://doi.org/10.1007/s00710-024-00867-0

RESEARCH

On thorite in Nubian granodiorite (Southwestern Egypt)

Kamaleldin M. Hassan[1]

Received: 1 April 2024 / Accepted: 12 July 2024

Abstract
Thorite, as a principally thorium (Th)-bearing mineral, is an important indicator for Th mineralization. However, its occurrence and enrichment processes are still discussed and debated. Here, a unique occurrence of thorite, discovered in Nubian granodiorite rather than in highly evolved granites from southwestern Egypt, is reported. This report presents data derived from optical and backscattered electron (BSE) microscopy and energy-dispersive X- ray spectrometry (EDS) analyses conducted on the thorite and its host rock. The Nubian granodiorite thorites are viewed as secondary, not primary products. Two distinct types of secondary thorites are identified that are referred to as type A thorite and type B thorite herein. Type A thorite occurs as small grains that are enclaved in a fine-grained matrix of altered oligoclase and ferrohornblende, and clinochlore. Thorite grains, up to 100 µm in size are characterized by corona-type structures comprising of clinochlore and hematite with some barite. Their sources are most likely hydrothermal solutions occurring during an alteration stage and having relatively high conditions of sulfate activity. Type B thorite, on the other hand, forms crystallites in altered domains of magmatic allanite-(Ce), ranging in size from ~0.1 to ~10 µm. Formation of Type B thorite is a direct result of fluid-driven alteration processes, since it requires the in situ-redistribution of elements, particularly thorium, silicon, and uranium. Thorite types A and B are composed mainly of thorium uranium silicate, with variable minor amounts of Y, Al, Ce, Nd, Fe, Ca, Na, Mg, P, and Cl. Thorite compositions are within the range reported for uranothorites from other occurrences.

Keywords Peraluminous granodiorite · Petrography · Secondary thorite · Allanite-(Ce)

Introduction

Thorite is thorium silicate ($ThSiO_4$) that crystallizes in the tetragonal system. It is a common member of the Th minerals which also include huttonite (monoclinic $ThSiO_4$), thorogummite [$(Th(SiO_4)_{1-x}(OH)_{4x})$], uranothorite [(Th, U)$SiO_4$)], ferrothorite [(Th, Fe)SiO_4)], orangite [($ThSiO_4$) H_2O)], thorianite (ThO_2), thorutite [(Th, U,Ca)Ti_2(O, $OH)_6$], and brockite [(Ca, Th, Ce)(PO_4)(H_2O)]. The tetragonal thorite forms a lower P-T than its monoclinic dimorph huttonite (Finch et al. 1964) that is considerably less common. Thorite, unlike huttonite, occurs mostly in the metamict state (Farges and Calas 1991). Metamictization and hydration of thorite lead to the loss of radiogenic Pb, yielding younger apparent ages (von Blanckenburg 1992). In natural samples, thorite ($ThSiO_4$) forms extensive solid solutions with other tetragonal minerals including zircon ($ZrSiO_4$), xenotime (YPO_4), and coffinite ($USiO_4$) (Förster 2006). However, the extent range of solid solution between the hydrous varieties of thorite + zircon and thorite + coffinite is less than 10 mol% (Mumpton and Roy 1961) and, hence, raises doubts on the stability of the intermediate members of the tetragonal system (Förster 2006).

Natural occurrences of thorite have been described from a wide range of geological environments including, but they are not limited to, (1) felsic igneous rocks (Hetherington and Harlov 2008; Hirtopanui et al. 2013; Abu Zeid 2014; Vasilatos and Papoutsa 2023), (2) metasediments (Speer 1982; Bingen et al. 1996; Franz et al. 1996), (3) ore deposits (Chen et al. 2022; Sun et al. 2024), and (4) fault zones in granitic plutons (Kamineni and Lemaire 1991). Thorite may count for up to 50 wt% of the Th, 20 wt% of the U, and

Editorial handling: X. Xu

✉ Kamaleldin M. Hassan
kamaleldin.hassan@nma.org.eg

[1] Division of Research, Nuclear Materials Authority, El Katameya, New Cairo 3, Cairo Governorate 4710030, Egypt

Published online: 26 August 2024

10 wt% of the bulk-rock heavy rare earth elements (HREE) and Y in weakly peraluminous granites (Förster 2006). In peralkaline, metaluminous-, and peraluminous-A type granites, up to 40 wt% of the Th and 20 wt% of the U contents may reside within thorite (Bea 1996). Although thorite is the most common Th mineral in nature, it is not the primary ore of thorium. The phosphate mineral monazite is mined for thorium and REE. If monazite deposits become scare or the demand for Th increases, then thorite and to a lesser extent, the other Th minerals will gain great importance. Currently, uranothorite is an important ore for U production (Hirtopanu et al. 2013).

Thorite forms inclusions in many minerals including zircon (Pointer et al. 1988; Hassan and Brunarska 2023), xenotime and monazite (Hetherington and Harlov 2008), allanite-group minerals (Buda and Nagy 1995; Guha et al. 2020; Zhang et al. 2023), and bastnäsite (Gieré et al. 1998). It also occurs as primary grains in hard rock (Förster 2006). Thorite enrichment and its occurrences commonly found in granites that are highly fractionated (Ragland et al. 1967; Pagel 1982; Bea 1996). The author here reports on the unique occurrence of thorite in a granodiotite from the basement complex, southwestern Egypt. Transmitted-light and BSE microscopy and EDS analyses were performed on the thorite and its host rock. My goal is to characterize thorite in these samples and to assess its sources. Thorite sources seem to be controlled by secondary, rather than primary, processes. These findings should provide clarification on why thorite may occur in less fractionated felsic rocks rather than in highly evolved granites.

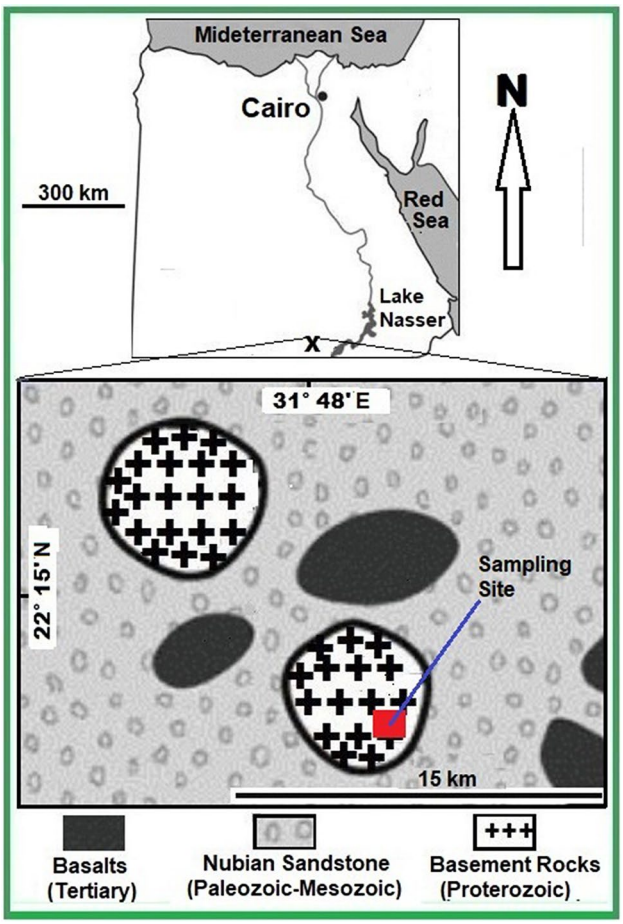

Fig. 1 Geological map of southwestern Egypt (revised from GSMA 1981)

Geological background

The Nubian granodiorite forms part of ~20 km^2 basement complex that is exposed at two adjacent sites in southwestern Egypt (Fig. 1) and also includes granites, tonalities, and monzodiorites. Tectonically, it is related to the tonalite-granodiorite magma, emplaced in succeeding phases, containing amphiboles (hornblende), micas (biotite) or both during the Proterozoic (Sabet 1972; List et al. 1989). The basement complex rocks occur in the forms of small knobs and residual boulders partially covered with sand that forms the country rocks in the entire region of southwestern Egypt. The knobs and boulders are the remnants of a mountain succumbed to desert erosion which is evident from the large accumulations of rock debris and granite-derived soil in the studied two sites. The soil does not have a developed profile and is largely medium to coarse-grained. Mineralogically, it comprises quartz, albite, illite, aluminous hematite, vermiculite, chlorite, and biotite (Hassan and Gunnlaugsson 2013). Present-day climatic conditions are hot summers and rains occurring on rare occasions.

Petrography of the Nubian granodiorite and its associated granites has demonstrated that these samples have characteristic REE accessory minerals. These are: (1) allanite-(Ce) in the Nubian granodiorite (Hassan 2008) and britholite-(Ce) in the granites (Hassan 2023). Chemical (major) analyses of two representative samples of the Nubian granodiorite are reported by Hassan (2008) and only a brief summary of the results is given here. The samples, namely S1 and S2 have a high acidic signature (SiO_2 = 72.5 wt%). They are peraluminous, with values of peralkalinity index [PAI = mol $Na_2O + K_2O/Al_2O_3$] = 0.77, Al saturation index [(ASI = mol $Al_2O_3/(CaO - (3.33 \times P_2O_5) + Na_2O + K_2O)$] = 1.1, and $corundum_{normative}$ = 0.89. The peraluminous character suggests possible S-type source similar in this respect to some granitoids of the Eastern Desert, Egypt (Abu El-Leil 1980). S-type granitiods originate from a sedimentary source involving the removal of sodium into sea or evaporites and calcium into carbonates, and therefore, relative enrichment of the source in Al occurs (Mc Birney 1993). However, origin of the Nubian granodiorite by a sedimentary source is not consistent with the contents of Na_2O and

K_2O of the samples falling within the igneous-type source field of the Chappell and White (1974) granite classification (not shown). It is also inconsistent with the presence of magmatic allanite-(Ce) as well as the absence of both garnet and endogenic xenoliths in these samples.

Sampling and analysis

Samples S1 and S2 of the Nubian granodiorite, previously studied by Hassan (2008) were used for the present research. They are fine to medium-grained, light grey, and exhibit slightly gneissose texture, where lighter minerals are thicker than the mafic ones that constitute thin streaks. Powder X-ray diffraction (XRD) analysis of the two samples was made using a Philips PW 1710 diffractometer. In these samples, besides major quartz and feldspar, ferrohornblende was identified by XRD as the main iron component: it is associated with minor amounts of clinochlore. Thin section of the samples S1 and S2 were prepared and studied by conventional optical methods in transmitted and reflected light using a polarizing microscope Olympus BX41 equipped with a digital camera. In addition, selected minerals in carbon-coated thin sections were analyzed using a field emission-scanning electron microscope (FE-SEM, Hitachi S-4700) attached to Norman Vantage EDS. FE-SEM operation conditions are: accelerating voltage = 20 kV, working distance = 1.2 cm, beam current = 10 µA and counting time = 100 s. The correction procedure Phi-Rho-Z was employed for raw data. The accuracy of the results was checked through analyzing duplicate mineral spots. The analytical errors of SEM-EDS method (standard deviation from duplicate samples) were < 5% for major elements and up to 40% for trace elements.

For whole-rock minor chemical analysis, aliquots of the Nubian granodiorite samples S1 and S2 (0.20 g) were mixed with a flux of lithium tetraborate ($LiBO_2$)/metaborate ($Li_2B_4O_7$), and then fused in a furnace at 1050°C. The cooled bead was dissolved in a 5% nitric acid (HNO_3) solution. The dissolved mixture was taken up in 1% HNO_3 and then analyzed by a Perkin Elan inductively coupled plasma-mass spectrometer (ICP-MS). The analyzed elements were Rb, Sr, Ba, Y, Zr, Th, U, La, Ce, Pr, Nd, Sm, Eu, Gd, Tb, Dy, Ho, Er, Tm, Yb, and Lu. The accuracy of these analyses was monitored by the use of standard materials (OREAS45E, OREAS24P, SO-18, DOLOMITE-2), analysis of reagent blanks, and replicate analyses. The analytical errors (standard deviation determined from different sample duplicates) were 5–9%. For comparison, samples of the leucocratic and biotite granites associated with the Nubian granodiorite were analyzed for 21 minor elements (Rb, Sr, Ba, Y, Zr, Th, U, La, Ce, Pr, Nd, Sm, Eu, Gd, Tb, Dy, Ho, Er, Tm, Yb, and Lu) using the ICP-MS method described above.

Results

Microscopy and textural characteristics

Host rock

The Nubian granodiorite, under optical microscope, is consisted of quartz, plagioclase, and potash feldspar, with a minor amount of ferrohornblende (Fig. 2). The ferrohornblende forms cleavable streaks arranged in parallel directions along the gneissosity planes and is partially altered to clinochlore. Quartz occurs as small grains filling the interstitial spaces between other minerals, and also as medium to large crystals showing wavy extinction and few suture

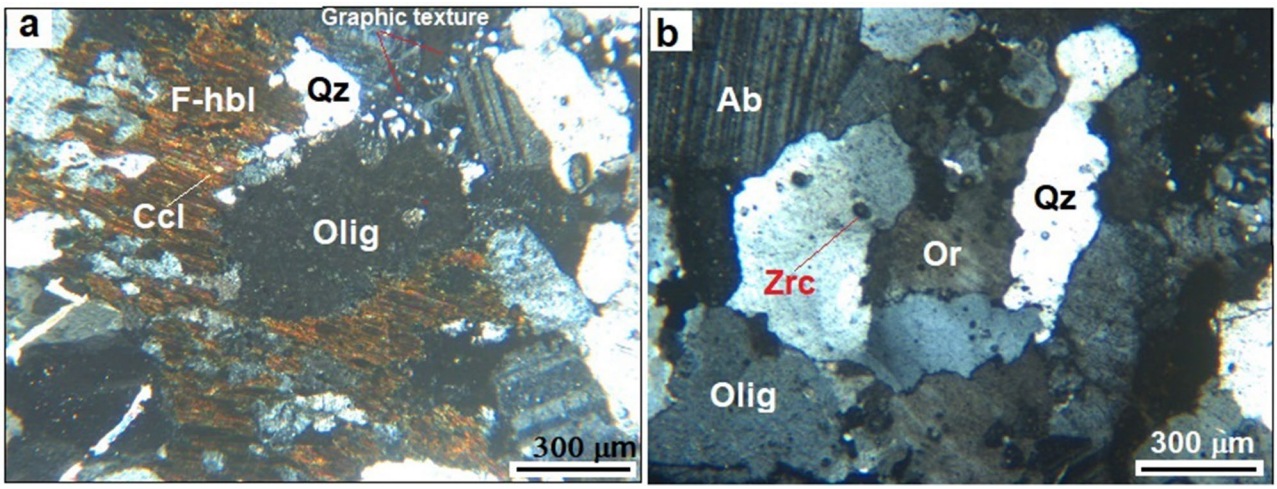

Fig. 2 (**a**–**b**) Cross-polarized transmitted-light images show the textural and mineral composition of samples collected from the Nubian granodiorite. Mineral abbreviations: Ab—albite, Ccl—clinochlore, F-hbl—ferrohornblende, Olig—oligoclase, Or—orthoclase, Qz—quartz, Zrc—zircon

edges. The plagioclase is represented by albite and oligoclase, forming phyenocrysts partially altered to epidote and to a greater extent sericite. The K-feldspar, mainly orthoclase has a cloudy appearance and is partially replaced by clay. The accessory minerals found in the studied samples are: thorite < zircon < allanite-(Ce). Scare barite found in these samples forms crystallites up to 20 μm in length.

Thorite

Thorite occurs as small grains in a fine-grained matrix consisting of altered plagioclase (mainly oligoclase) and ferrohornblende, varying in size from ~20 to ~100 μm (Fig. 3a and b). Optically, it is nearly opaque and, in plane polarized light, appears yellow-orange. On the BSE image, thorite grains exhibit characteristics of undeformed crystals surrounded by corona-type structures comprising clinochlore and hematite, with some barite (Fig. 3c and d).

Representative EDS elemental data of thorite grains in Fig. 3 are provided in Table 1. Thorite major constituents are Th, Si, and to a lesser extent U. The minor constituents, on the other hand, are: Al_2O_3, Y_2O_3, Ce_2O_3, Nd_2O_3, Fe_2O_3, CaO, MgO, P_2O_5, Na_2O, and Cl.

Allanite-(Ce)

Allanite-(Ce) occurs as euhedral to subhedral crystals in a fine-grained plagioclase matrix in the samples (Fig. 4a and b). The size of allanite-(Ce) grains can be up to 1100 μm as observed in thin sections. Most of the allanite-(Ce) crystals examined are highly affected by post-magmatic transformations. Petrographic observations indicate that allanite-(Ce) show dissolution-reprecipitation textures. The altered regions of allanite-(Ce) appear darker in BSE images than the unaltered ones (Fig. 4c–f). Furthermore, alteration of allanite-(Ce) is characterized by the partial replacement by thorite, clay, epidote, britholite-(Ce), and others. The thorite

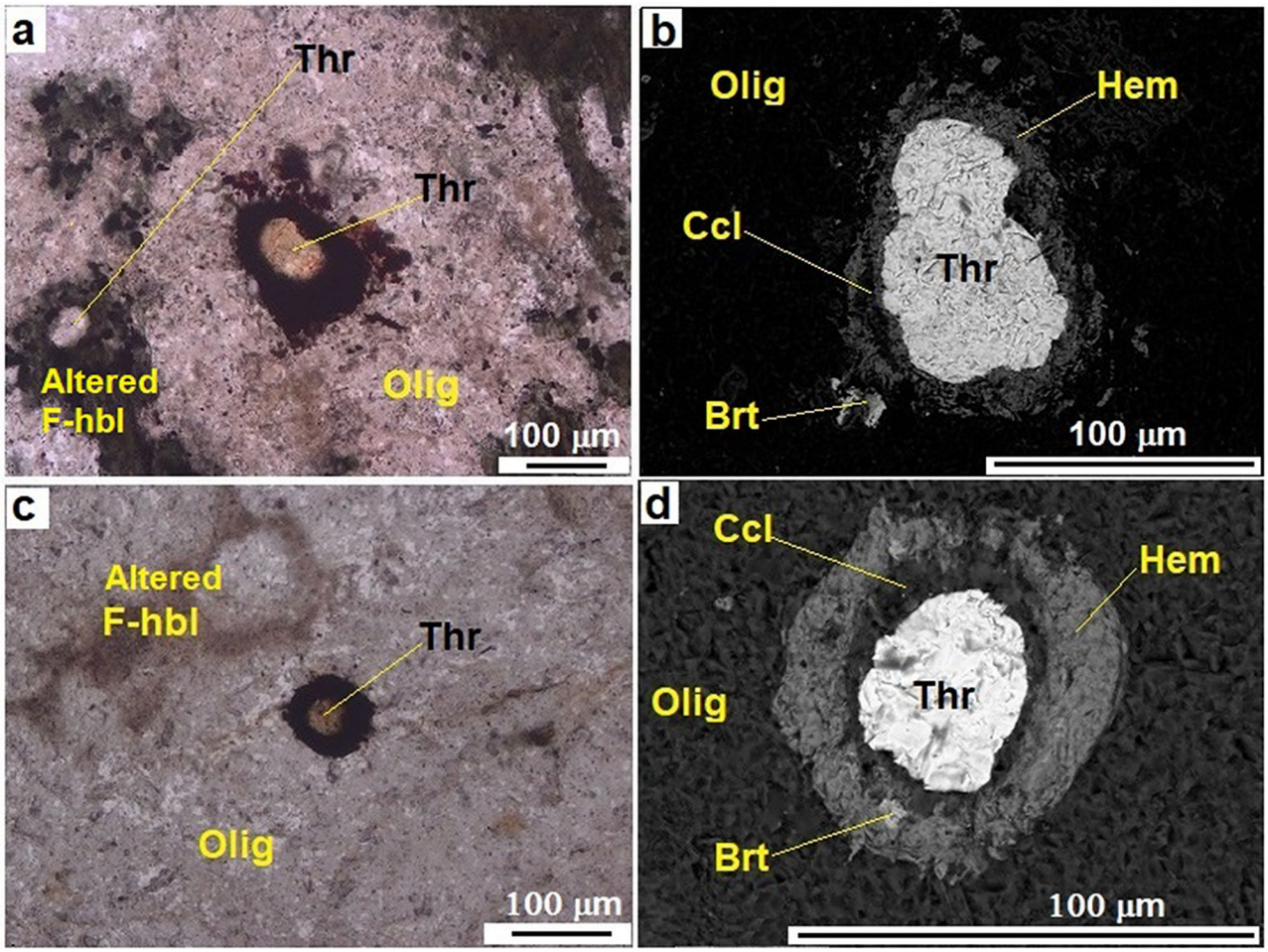

Fig. 3 Plane-polarized transmitted-light (a, c) and BSE images (b, d) of thorite grains from the Nubian granodiorite. **a** Euhedral (lower left) and kidney-shaped grains (center) in altered oligoclase and ferrohornblende. **b** Detail enlargement showing the kidney shaped grain (center) depicted in (**a**). **c** Subrounded grain in altered oligioclase. **d** Same grain as in (**c**), detail enlargement. Mineral abbreviations not yet identified are: Brt—barite, Hem—hematite, Thr—thorite

Table 1 Representative EDS quantitative chemical data (wt%) from the Nubian granodiorite, southwestern Egypt

	#	SO_3	P_2O_5	SiO_2	TiO_2	UO_2	ThO_2	Al_2O_3	Y_2O_3	La_2O_3	Ce_2O_3	Pr_2O_3	Nd_2O_3	Sm_2O_3	F
Thorite[a]	1	BDL	BDL	22.43	BDL	10.90	53.80	1.64	5.70	BDL	1.25	BDL	1.20	BDL	BDL
	2	BDL	BDL	23.11	BDL	12.10	52.30	1.76	5.62	BDL	1.20	BDL	1.07	BDL	BDL
	3	BDL	BDL	21.62	BDL	11.40	53.50	1.58	5.36	BDL	1.03	BDL	1.00	BDL	BDL
	4	BDL	BDL	21.28	BDL	12.90	53.10	1.63	5.52	BDL	1.13	BDL	0.92	BDL	BDL
	5	BDL	0.61	23.58	BDL	15.20	45.90	1.98	7.72	BDL	0.47	BDL	0.69	BDL	BDL
	6	BDL	0.74	18.18	BDL	16.60	51.10	1.67	3.78	BDL	1.36	BDL	0.91	BDL	BDL
	7	BDL	1.6	25.69	BDL	5.52	53.80	2.86	BDL	BDL	0.99	BDL	0.42	BDL	BDL
	8	BDL	BDL	23.20	BDL	6.89	51.70	1.87	5.57	BDL	BDL	BDL	0.91	BDL	BDL
	9	BDL	BDL	16.66	BDL	20.40	49.30	1.70	5.17	BDL	1.03	BDL	0.79	BDL	BDL
	10	BDL	1.11	23.81	BDL	17.30	52.40	1.84	BDL	BDL	BDL	BDL	BDL	BDL	BDL
	11	BDL	0.71	21.37	BDL	19.20	52.10	1.67	BDL	BDL	BDL	BDL	0.78	BDL	BDL
	12	BDL	0.62	18.61	BDL	19.40	53.60	1.65	BDL	BDL	0.93	BDL	0.68	BDL	BDL
	13	BDL	2.27	32.62	BDL	BDL	51.40	5.57	BDL	BDL	1.14	BDL	BDL	BDL	BDL
Clinochlore	1	BDL	BDL	39.42	BDL	BDL	BDL	16.75	BDL	BDL	BDL	BDL	BDL	BDL	BDL
Hematite	1	BDL	BDL	1.85	2.78	BDL	BDL	0.66	BDL	BDL	BDL	BDL	BDL	BDL	BDL
Barite	1	30.40	BDL	6.36	BDL	BDL	BDL	2.13	BDL	BDL	BDL	BDL	BDL	BDL	BDL
Oligoclase	1	BDL	BDL	64.22	BDL	BDL	BDL	22.45	BDL	BDL	BDL	BDL	BDL	BDL	BDL
Zircon	1	BDL	BDL	29.14	BDL	0.16	BDL	BDL	BDL	BDL	BDL	BDL	BDL	BDL	BDL
	2	BDL	BDL	28.78	BDL	0.04	0.06	0.34	BDL	0.62	1.34	BDL	BDL	BDL	BDL
Inclusions in Zircon	1	BDL	BDL	18.51	BDL	BDL	BDL	1.57	BDL	13.97	22.76	BDL	4.54	BDL	BDL
	2	BDL	BDL	11.02	BDL	BDL	BDL	2.17	BDL	20.9	35.69	BDL	7.06	BDL	BDL
Allanite-(Ce)															
Unaltered	1	0.62	BDL	32.85	BDL	BDL	5.08	12.02	BDL	4.78	15.84	1.08	5.68	BDL	BDL
	2	BDL	BDL	32.85	BDL	BDL	3.08	13.88	BDL	4.95	13.59	BDL	3.97	BDL	BDL
	3	BDL	BDL	29.29	BDL	BDL	BDL	11.05	BDL	5.65	21.7	BDL	6.51	BDL	BDL
	4	1.24	BDL	32.77	BDL	BDL	7.14	10.51	BDL	4.60	18.10	2.15	7.57	BDL	BDL
Altered	1	BDL	BDL	39.02	BDL	BDL	BDL	13.45	BDL	9.44	18.77	5.39	BDL	0.80	0.77
	2	BDL	BDL	44.20	BDL	BDL	BDL	15.11	BDL	7.68	15.44	BDL	4.19	0.85	1.13
	3	BDL	BDL	50.07	0.98	BDL	BDL	17.96	BDL	1.99	6.33	BDL	2.89	BDL	BDL
Alteration products of Allanite-(Ce)															
Thorite[b]	1	BDL	BDL	28.53	BDL	BDL	51.90	5.69	BDL	1.74	3.68	BDL	1.55	BDL	BDL
	2	BDL	BDL	23.32	BDL	5.43	65.22	2.21	BDL	BDL	BDL	BDL	BDL	BDL	BDL
	3	BDL	BDL	28.22	BDL	BDL	38.59	7.65	BDL	1.53	4.39	BDL	2.55	BDL	BDL
	4	BDL	BDL	28.38	BDL	BDL	45.24	6.67	BDL	1.63	4.03	BDL	2.05	BDL	BDL
Britholite-(Ce)	1	BDL	BDL	18.22	BDL	BDL	3.86	6.73	BDL	15.09	35.38	BDL	8.47	BDL	BDL
REE Oxide	1	BDL	BDL	5.37	BDL	BDL	4.12	1.99	0.47	19.04	45.99	4.70	12.82	BDL	BDL
Hematite	1	BDL	BDL	1.94	2.92	BDL	BDL	0.97	BDL	BDL	BDL	BDL	BDL	BDL	BDL
Epidote	1	BDL	BDL	36.96	0.65	BDL	BDL	10.1	BDL	BDL	BDL	BDL	BDL	BDL	BDL
Clay	1	0.24	BDL	52.10	0.06	BDL	BDL	20.24	BDL	BDL	BDL	BDL	BDL	BDL	BDL

Table 1 (continued)

	#	Gd_2O_3	MgO	CaO	BaO	MnO	Fe_2O_3	Na_2O	K_2O	Ag_2O	MoO_2	ZrO_2	HfO_2	Cl	Total
Thorite[a]	1	BDL	BDL	1.83	BDL	BDL	1.26	BDL	BDL	BDL	BDL	BDL	BDL	BDL	100.01
	2	BDL	BDL	1.71	BDL	BDL	1.15	BDL	BDL	BDL	BDL	BDL	BDL	BDL	100.02
	3	BDL	BDL	1.75	BDL	BDL	1.93	0.54	BDL	BDL	BDL	BDL	BDL	0.30	100.01
	4	BDL	BDL	1.80	BDL	BDL	1.73	BDL	BDL	BDL	BDL	BDL	BDL	BDL	100.01
	5	BDL	BDL	1.51	BDL	BDL	1.76	0.61	BDL	BDL	BDL	BDL	BDL	BDL	100.03
	6	BDL	BDL	2.51	BDL	BDL	2.08	1.14	BDL	BDL	BDL	BDL	BDL	BDL	100.07
	7	BDL	BDL	2.59	BDL	BDL	5.04	1.12	BDL	BDL	BDL	BDL	BDL	0.40	100.03
	8	BDL	BDL	4.28	BDL	BDL	4.71	0.58	BDL	BDL	BDL	BDL	BDL	0.28	99.99
	9	BDL	0.16	1.57	BDL	BDL	3.21	BDL	BDL	BDL	BDL	BDL	BDL	BDL	99.99
	10	BDL	BDL	1.21	BDL	BDL	1.52	0.82	BDL	BDL	BDL	BDL	BDL	BDL	100.01
	11	BDL	0.25	1.58	BDL	BDL	1.87	0.46	BDL	BDL	BDL	BDL	BDL	BDL	99.99
	12	BDL	BDL	1.40	BDL	BDL	2.35	0.68	BDL	BDL	BDL	BDL	BDL	BDL	99.92
	13	BDL	BDL	2.95	BDL	BDL	2.44	1.61	BDL	BDL	BDL	BDL	BDL	BDL	100.0
Clinochlore	1	BDL	10.22	0.31	BDL	0.39	29.57	1.15	1.84	BDL	BDL	BDL	BDL	0.35	100.0
Hematite	1	BDL	BDL	BDL	BDL	BDL	94.37	0.35	BDL	BDL	BDL	BDL	BDL	BDL	100.01
Barite	1	BDL	BDL	1.11	56.86	BDL	0.67	2.08	0.40	BDL	BDL	BDL	BDL	BDL	100.01
Oligoclase	1	BDL	BDL	6.82	BDL	BDL	BDL	5.89	0.63	BDL	BDL	BDL	BDL	BDL	100.01
Zircon	1	BDL	BDL	BDL	BDL	BDL	BDL	BDL	0.16	BDL	BDL	68.03	2.50	BDL	99.99
	2	BDL	BDL	BDL	BDL	BDL	BDL	0.33	0.16	BDL	BDL	66.44	1.91	BDL	100.02
Inclusions in zircon	1	BDL	BDL	3.66	BDL	BDL	3.47	0.86	0.41	BDL	BDL	30.23	BDL	BDL	99.98
	2	BDL	0.48	6.01	BDL	BDL	5.33	BDL	0.31	BDL	BDL	11.03	BDL	BDL	100.00
Allanite-(Ce)															
Unaltered	1	BDL	0.34	8.60	BDL	BDL	10.55	1.11	1.23	BDL	BDL	BDL	BDL	BDL	99.78
	2	BDL	0.69	10.68	BDL	BDL	15.11	0.79	0.47	BDL	BDL	BDL	BDL	BDL	100.06
	3	BDL	0.89	8.92	BDL	BDL	8.39	1.76	1.96	3.54	BDL	BDL	BDL	0.33	99.99
	4	BDL	BDL	6.49	BDL	BDL	6.00	1.44	1.99	BDL	BDL	BDL	BDL	BDL	100.00
Altered	1	1.13	BDL	6.66	BDL	BDL	BDL	3.72	0.88	BDL	BDL	BDL	BDL	BDL	100.03
	2	0.72	BDL	4.73	BDL	BDL	BDL	5.41	0.52	BDL	BDL	BDL	BDL	BDL	99.98
	3	BDL	BDL	6.34	BDL	BDL	7.79	BDL	2.76	2.67	BDL	BDL	BDL	0.23	100.01
Alteration products of Allanite-(Ce)															
Thorite[b]	1	BDL	BDL	2.14	BDL	BDL	4.09	0.68	BDL	BDL	BDL	BDL	BDL	BDL	100.0
	2	BDL	BDL	2.15	BDL	BDL	1.07	0.60	BDL	BDL	BDL	BDL	BDL	BDL	100.0
	3	BDL	BDL	8.37	BDL	BDL	8.02	0.69	BDL	BDL	BDL	BDL	BDL	BDL	100.01
	4	BDL	BDL	5.25	BDL	BDL	6.06	0.69	BDL	BDL	BDL	BDL	BDL	BDL	100.0
Britholite-(Ce)	1	BDL	1.07	5.19	BDL	BDL	3.30	1.24	1.21	BDL	BDL	BDL	BDL	0.23	99.99
REE Oxide	1	BDL	BDL	5.23	BDL	BDL	BDL	0.30	BDL	BDL	BDL	BDL	BDL	BDL	100.03
Hematite	1	BDL	BDL	BDL	BDL	0.18	93.58	0.41	BDL	BDL	BDL	BDL	BDL	BDL	100.0
Epidote	1	BDL	1.64	10.98	BDL	0.56	33.91	1.82	1.98	BDL	BDL	BDL	BDL	1.38	99.98
Clay	1	BDL	4.85	BDL	BDL	BDL	14.41	0.83	6.65	BDL	BDL	BDL	BDL	0.80	100.2

[a]Analytical results are shown in Fig. 3; [b]Analytical results are shown in Fig. 4; BDL—below detection limit

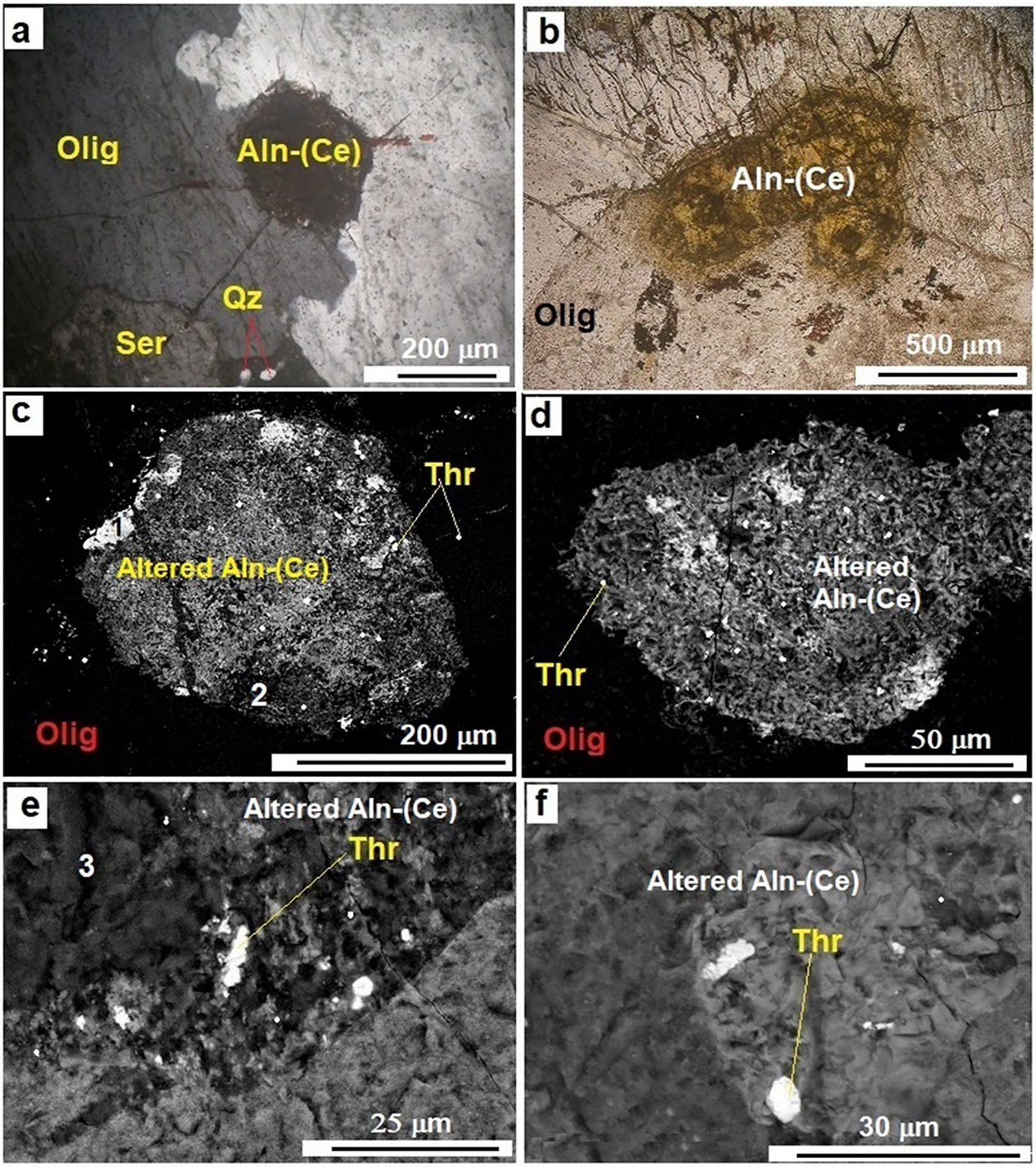

Fig. 4 Optical and BSE images of allanite-(Ce) grains from the Nubian granodiorite. **a** Cross-polarized transmitted-light image of euhedral grain showing some sign of alteration. **b** Plane-polarized transmitted-light image prismatic grain showing excessive alteration. The grains of both (**a**) and (**b**) images are associated with oligoclase and are characterized by radial cracks extending out into the surrounding minerals. **c-f** BSE images of altered allanite-(Ce) grains partially replaced by secondary thorite (bright spots) and other secondary minerals. Points in images: 1—britholite-(Ce); 2—LREE-silicate; 3—clay. Aln-(Ce)—allanite-(Ce), Ser—sericite

occurs in or near altered regions of allanite-(Ce), forming crystallite agglomerations ranging from ~0.1 to ~10 µm. Thorite crystallites, on BSE images, appear as bright spots (Fig. 4c–f). The crystallites are obvious in these images: because the mean atomic number of thorite is high, it appears bright. Their sizes and distributions vary across the hosting allanite-(Ce); areas of alterations contain more but smaller thorites.

Representative EDS elemental data of thorites shown in Fig. 3 are listed in Table 1. Thorite major constituents are Th, Si, and to a lesser extent U, with minor amounts of Al_2O_3, La_2O_3, Ce_2O_3, Nd_2O_3, Fe_2O_3, CaO, and Na_2O.

Zircon

In the Nubian granodiorite, zircon is abundant as euhedral gains ranging in size from ~60 to ~100 µm, showing embayment corrosion, and containing inclusions of light rare earth elements (LREE). Small zircon grains are often included within plagioclase and quartz, suggesting a wide range of zircon crystallization during the solidification of the parent magma. The elemental compositions of zircon are close to pure (Zr, Hf) silicate (Table 1), suggesting the EDS method employed in this study is satisfactory.

ICP-MS results

The ICP-MS analytical results are provided in the online electronic supplementary material (ESM; Table S1). The Nubian granodiorite samples S1 and S2 have less U and more Y, Th, and REE than the leucocratic or biotite granite. They are characterized by a strong negative europium anomaly (Eu/Eu* = 0.22–0.25). This may reflect high oxidation conditions (Rudnik and Gao 2003) or could also be inherited from magma sources (Khoshnoodi et al. 2017).

The Nubian granodiorite Th/U ratios exceed the range 3–4 expected for primary igneous rocks (Keevil 1944; Wedepohl 1995). Higher Th/U ratios reflect the retention of Th and release of U, which likely occurred as a result of oxidizing conditions. Under oxidation influence U forms the uranyl ion (UO^{2+}_2) in which U has a valence of +6. The UO^{2+}_2 form compounds that are soluble in solution. Therefore, U is mobile element under oxidizing conditions and is separated from Th which exists as tetravalent ion and whose compounds are generally insoluble in solution. Mobilization of UO^{2+}_2 is associated with fluorine complexing at high temperature conditions (Kimberley 1978; Keppler and Wyllie 1990).

Discussion

Thorites may form at an early magma stage (Vasilatos and Papoutsa 2023) or from late- to post-magmatic (pegmatite and hydrothermal) fluids (Hirtopanui et al. 2013; Sun et al. 2024). Magmatic thorites should have well-crystallized shapes like prismatic zircons or have distinct straight boundaries. These characteristics are absent in thorites of the Nubian granodiorite. Thus, the Nubian granodiorite thorites would have grown from secondary aqueous solutions rather than magmatic melts. In Fig. 3, thorite grains are enclaved in the oligoclase that was polycrystalline and experienced obvious and heavy alteration. The enclavation of thorite grains in these oligoclase domains would suggest that these grains were precipitated during an alteration stage. Thorite grains show characteristics of underformed crystals that are surrounded by well-preserved, corona-type structures comprising clinochlore and hematite, with some barite. The corona structures (excluding clinochlore) suggest that the thorite crystallized under relatively high conditions of oxygen fugacity (fO_2) and sulfate (SO_4^{2-}) activity (Kamineni and Lemire 1991. The inferred fO_2 and SO_4^{2-} conditions point to hydrothermal solutions. The SO_4^{2-} ions might be involved in the transportation of Th. Si, U, and other elements necessary for the nucleation and crystallization of thorite (Sun et al. 2024). The clinochlore found around thorite (Fig. 3) was a typically alteration mineral which formed from ferrohornblende, as indicated from the petrography. Its presence supports the contention that the thorite was precipitated in cavities during alteration processes.

The thorite (Fig. 3) appears remarkably unalterd—a feature that has been reported for thorite in granites (Kamineni and Lemire 1991; Förster 2006). Generally, thorite is more stable in geological environments than other actinide minerals. This is simply because thorium (as thorite) exists in only one oxidation state (Th^{4+}) that is essentially immobile in solution. The tetravalent Th^{4+} cation does not undergo either oxidative dissolution as occurs for uranium (U^{4+}) or reductive dissolution as could occur for plutonium (Pu^{4+}) (Cleveland 1979). Furthermore, the intensity of radioactivity of Pu^{4+}, for example, could cause damages to the host material. However, for most conditions in a nuclear fuel waste burial chamber, the tetravalent actinide oxides are relatively stable (Lemire and Garisto 1989). Thorium, which is about three times as common as uranium in the earth's crust (Rudnik and Gao 2003), could be used as a replacement for uranium in nuclear power generation. Th-based nuclear wastes are characterized by fewer radioactive elements than other conventional radioactive elements such as uranium (van Gosen et al. 2009), which led to worldwide attentions on Th resource exploration.

The partial chemical alteration of allanite-(Ce) and subsequent formation of thorite in the altered domains (Fig. 4) is a direct result of dissolution-reprecipitation processes. These processes must have occurred in an effectively closed-chemical system, i.e., Th, Si, U, and other elements necessary for the nucleation and growth of thorite were already present in the host allanite-(Ce). As the dissolution of the allanite-(Ce) continues, the interface between the fluid and solid migrates as it is replaced by the new mineral phase (thotite). Interconnected pore spaces allow infiltration of fluids and thus aid the transport of the Th, Si, U, and others near or within the altered regions of the allanite-(Ce). Transport of these elements by fluids requires complexing the cations. Anions commonly involved for complexing include CO_3^{2-}, SO_4^{2-}, HPO_4^{2-}, Cl^-, and F^-. Although anion contents are not available in bulk analyses, the EDS analysis indicates that fluorine, chlorine, and sulfate are present in the samples (Table 1). Fluorine and SO_4^{2-} are though to be important for complexing Th, U, REE, and other elements during the alteration of allanite (Zhang et al. 2023).

The alteration of allanites is likely linked to metamictization of the samples (Morin 1977; Wood and Richetts 2000). Metamictization occurs as result of α-decay-event recoil following radioactive decay of a U or Th atom contained in a crystalline material. The recoiled particles travel a distant equivalent to a few unit cells, causing damages of the host mineral and, in some cases, can destroy its crystal lattice completely while leaving the outward appearance intact. These damaged zones are susceptible to dissolution and removal by fluids, leaving behind pore spaces. Here, the secondary thorite and porosity increase in altered domains of allanite-(Ce) (Fig. 4). Therefore, recoil induced by radioactive decay should be considered as a mechanism favoring porosity formation in the Nubian granodiorite allanite-(Ce). However, in other studies, porosity was only observed in altered domains of xenotime and monazite that have lower concentrations of Th and U (Hetherington and Harlov 2008). Therefore, radiation damage by radioactive decay in accessory minerals cannot by itself be responsible for the development of porosity in these samples. In contrast, porosity tends to be a result of secondary chemical alteration, typically resulting in some loss of material.

A review of results of chemical analyses of thorite from other studies indicates the presence of as much as 40 elements (Speer 1982). In contrast, in the present study evidence for only 13 elements is obtained (Table 1); the rest are either absent or present in amounts below the detection limit of the EDS method. ThO_2, SiO_2, and UO_2 constitute the major components in the thorites of the Nubian granodiorite. These compositions correspond to thorium uranium silicate (Th, U)SiO_4. The highest reported contents of U in thorite from granites were from Nigeria (~29 wt% UO_2; Pointer et al. 1988) and Germany (~23 wt% UO_2; Förster 2006). The Nubian granodiorite thorites contain ca. 5–21 wt% UO_2 (Table 1). The Nubian granodiorite thorites contain variable small amounts of non-formula elements including Y_2O_3, Al_2O_3, Ce_2O_3, Nd_2O_3, Fe_2O_3, CaO, Na_2O, MgO, P_2O_5, and Cl. The entry of such elements into thorite is common in natural samples (Speer 1982; Pointer et al. 1988; Žáček et al. 2009; Hassan and Brunarska 2023). This is assigned to the interaction between the metamict mineral and hydrothermal fluids. Thorites from granites always contain several wt% of REE, with a strong predominance of HREE over LREE (Bea 1996; Förster 2006). The REE patterns of thorite from Czech Republic, however, show enrichments in LREE over HREE (Žáček et al. 2009). In the present study, the content of heavy REE was found to be below the detection limit of EDS chemical analysis.

The chemical compositions of thorites vary widely depending on the chemistry of the environment of formation and reflect complex solid solutions with other minerals. Förster (2006) described a complete solid solution between zircon ($ZrSiO_4$), thorite ($ThSiO_4$) + coffinite ($USiO_4$), and xenotime [(Y, REE)PO_4)]. In the thorites of the Nubian granodiorite, the components U, Y, Ce, Fe, and Ca are hence assumed to replace Th according to the following substitutions:

$$(\mathrm{REE, Y})^{3+} + \mathrm{Fe}^{3+} + \mathrm{U}^{6+} \rightleftarrows 3\mathrm{Th}^{4+} \quad (1)$$

$$2\mathrm{Ca}^{2+} \rightleftarrows \mathrm{Th}^{4+} \quad (2)$$

The presence of P_2O_5 in the Nubian granodiorite thorites may suggest the following substitution:

$$\mathrm{REE}^{3+} + \mathrm{P}^{5+} \rightleftarrows \mathrm{Th}^{4+} + \mathrm{Si}^{4+} \quad (3)$$

Sulfur identified in thorites from other studies probably substitutes for Si (Speer 1982), and in the present case it is below the EDS detection limit.

The geochemical behavior of radioactive and rare elements in differentiated granitoids changes with aluminum saturation. Generally, the higher the ASI, the strong depletion in Th, U, REE (except Eu), and Y (Bea 1993). However, the Nubian granodiorite with higher ASI values (peraluminous) contain more Th, REE (except Eu), and Y than the associated leucocratic and biotite granites that have low ASI values (metaluminous). Had magmatic differentiation been responsible for the element contents, the Nubian granodiorite, which is peraluminous, should have less Th, REE and Y concentrations than the other two rocks that are metaluminous and more fractionated. The relative increases of these elements in the Nubian granodiorite are unrelated to some processes of differentiation such as crystallization

fractionation, but they are correlated with the presence of allanite-(Ce). The occurrence of thorite in granodiorite rather than granites in this study is related to allanite-(Ce) mineralizations and secondary processes.

Conclusions

The current study presents petrographical and mineralogical investigations of thorite in the Nubian granodiorite from the basement complex, southwestern Egypt. The results provide new data concerning enrichment of thorium (as thorite) in granodiorite rather than in the more fractionated granites in the area. Thorite enrichment is related to secondary, not magmatic differentiation processes. Two distinct types of secondary thorites are recorded in this study.

Type A thorite occurs as discrete grains that are enclaved in altered plagioclases and are characterized by corona-type structures. These microfeatures comprise clinchlore, hematite and to a lesser extent barite. The close-spatial association of type A thorite with these minerals (except clinochlore) strongly suggests it grew from hydrothermal solutions having relatively high conditions of oxygen fugacity and sulfate activity. The clinochlore was a direct result of alteration of ferrohornblende. Its presence suggests that the type A thorite precipitated during an alteration stage.

Type B thorite of the Nubian granodiorite, on the other hand, forms crystallite agglomerations in altered domains of magmatic allanite-(Ce). Formation of thorite crystallites in these altered domains is demonstrated to be a result of dissolution-reprecipitation processes where fluids dissolved some parts of allanite-(Ce) grains. Dissolved elements, mainly Si, Th, and U moved via pores and then redeposited as thorite close or within the host mineral.

The two thorite types (A and B) are mainly composed of thorium uranium silicate plus minor amounts of Y, Al, Ce, Nd, Fe, Ca, Na, Mg, P and Cl. The main compositional variations found in these thorites are most likely related to solid solution substitution reactions. These are: (1) [(REE, Y) + Fe + U ⇄ 3Th], (2) [Ca ⇄ Th], and (3) [REE + P ⇄ Th + Si]. Thorite compositions are generally in agreement with those reported for uranothorites from other occurrences.

Supplementary Information The online version contains supplementary material available at https://doi.org/10.1007/s00710-024-00867-0.

Acknowledgements The author acknowledges the staff of the "Toshka Uranium Study and Evaluation Project", the Nuclear Materials Authority (NMA), Egypt for field assistance. Thanks are to Ehab Abu Zeid of the NMA for access to his petrography laboratory; Abdullah Ahmed of the Mineral Resources Authority, Egypt for XRD analysis; and Suise Woo of the Bureau Veritas Commodities, Canada, for ICP-MS analysis. Thanks to Irena Brunarska and Merek Michalik of the Institute of Geological Sciences (Jagiellonian University, Poland) for SEM analysis. Constructive comments of editor-in-chief Lutz Nasdala, handling editor Xisheng Xu, and two anonymous reviewers are gratefully acknowledged.

References

Abu El-Leil I (1980) Geology, petrography and geochemistry of some granitic rocks in the north part of the Eastern Desert of Egypt. PhD thesis, Al Azhar University, Cairo, Egypt, 294 pp

Abu Zeid EK (2014) Contribution to the radioactivity, mineralogy and REEs distribution in the granitoids of Gebel El Nekeiba, South Eastern Desert, Egypt. Nucl Sci Sci J 3:55–66

Bea F (1993) Aluminosity dependent fractionation patterns in differentiated granite-leucogranite systems. Trans Amer Geophys Union. p 343 (abstract)

Bea F (1996) Residence of REE, Y, Th and U in granites and crustal protoliths; implications for the chemistry of crustal melts. J Petrol 37:521–552

Bingen B, Demaiffe D, Hertogen J (1996) Redistribution of rare earth elements, thorium, and uranium over accessory minerals in the course of amphibolite to granulite facies metamorphism: the role of apatite and monazite in orthogneisses from southwestern Norway. Geochim Cosmochim Acta 60:1341–1354

Buda G, Nagy G (1995) Some REE-bearing accessory minerals in two types of Variscan granitoids, Hungary. Geol Carpath 46:67–78

Chappell BW, White A (1974) Two contrasting granite types (expanded abstract). Pac Geol 8:173–174

Chen J, Fan H, Meng Y, Wang S (2022) Geochemical properties and resource distribution of thorium. J South China Univ 36:52–57 (in Chinese with English abstract)

Cleveland JM (1979) Critical review of plutonium equilibria of environmental concern. In: Melchior DC, Bassett RL (eds) Chemical modeling of aqueous systems II. Am Chem Soc Symp Ser 416, Washington DC, pp 321–338

Farges F, Calas G (1991) Structural analysis of radiation damage in zircon and thorite: an X-ray absorption spectroscopic study. Am Min 76:60–73

Finch CB, Harris LA, Clark GW (1964) The thorite–huttonite phase transformation as determined by growth of synthetic thorite and huttonite single crystals. Am Mineral 49:782–785

Förster HJ (2006) Composition and origin of intermediate solid solutions in the system thorite–xenotime–zircon–coffinite. Lithos 88:35–55

Franz G, Andrehs G, Rhede D (1996) Crystal chemistry of monazite and xenotime from saxothuringian–moldanubian metapelites, NE Bavaria, Germany. Eur J Mineral 8:1097–1118

Gieré R, Williams CT, Braun M, Graeser S (1998) Complex Zonation Patterns in Monazite-(Nd) and Monazite- (Ce). International Mineralogical Association, 17th General Meeting, Toronto, Abstract Volume, p A84

GSMA (1981) Geological map of Egypt, scale 1:2,000,000. Geological survey and Mining Authority. Abbasyia, Cairo, Egypt

Guha DB, Raza A, Neogi S, Korakoppa MM (2020) Allanite-britholite bearing migmatite gneiss-amet granite and intrusive syenite-monzonite rocks of SW Rajasthan, India, and their REE potential. Episodes 43:665–687

Hassan KM (2008) Petrography, chemistry and radioactivity of granitoids at north Gebel Seri, South Western Desert, Egypt. Isot Radiat Res 40:615–629

Hassan KM (2023) Britholite-(Ce) from the metaluminous granite of SW Egypt. Mineralogia 54:11–17

Hassan KM, Brunarska I (2023) Thorite inclusions in zircon of the monzogranite, Lower Nubia, SW Egypt. Mineralogia 54:69–77

Hassan KM, Gunnlaugsson HP (2013) Characterization of barren, granitic soils from the nubian Desert (SW Egypt) by 57Fe Mössbauer spectroscopy. Mineralogia 44:39–51

Hetherington CJ, Harlov DE (2008) Metasomatic thorite and uraninite inclusions in xenotime and monazite from granitic pegmatites, Hidra anorthosite massif, southwestern Norway: mechanics and fluid chemistry. Am Mineral 93:806–820

Hirtopanu PA, Jakab GY, Andersen CJ, Fairhurst JR (2013) Thorite, thorogummite and xenotime-(Y) occurrence in Ditrau alkaline intrusive massif, East carpathians. Proc Romanian Acad Sci Seer B 15:111–131

Kamineni DC, Lemire RJ (1991) Thorite in fault zones of a granitic pluton, Atikokan, Canada: implications for nuclear fuel waste disposal. Chem Geol 90:133–143

Keevil B (1944) Thorium-uranium ratios in rocks and minerals. Am J Sci 242:309–321

Keppler H, Wyllie PJ (1990) Role of fuids in transport and fractionation of uranium and thorium in magmatic processes. Nature 348:531–533

Khoshnoodi K, Behzadi M, Gannadi-Maragheh M, Yazdi M (2017) Alkali metasomatism and Th-REE-mineralization in the Choghart deposit, Bafq district, Central Iran. Geologia Croatica 70:53–69

Kimberley MM (1978) High-temperature uranium geochemistry. Mineral. Assoc. Can Short Course Handb 3:101–104

Lemire RJ, Garisto F (1989) The solubility of U, np, Pu, Th and Tc in a Geological Disposal Vault for used nuclear fuel. Atomic Energy of Canada Limited Report, pp AECL–10009

List FK, El-Gaby S, Tehrani R (1989) The basement rocks in the Eastern and Western deserts and Sinai. In: Hermina M, Klitzsch E, List F (eds) Stratigraphic lexicon and explanatory note to the geologic map of Egypt 1:500000. General Petroleum Corporation, Cairo, Egypt, pp 33–56

Mc Birney AR (1993) Igneous petrology. Jones & Bartlett, Boston

Morin JA (1977) Allanite in granitic rocks of the Kenora-Vermilion Bay Area, Northwestern Ontario. Can Mineral 15:297–302

Mumpton FA, Roy R (1961) Hydrothermal stability studies of the zircon-thorite group. Geochim Cosmochim Acta 21:217–238

Pagel M (1982) The mineralogy and geochemistry of uranium, thorium, and rare-earth elements in two radioactive granites of the Vosges, France. Mineral Mag 46:149–160

Pointer CM, Ashworth JR, Ixer RA (1988) The zircon– thorite mineral group in metasomatized granite, Ririwai, Nigeria 2. Zoning, alteration and exsolution in zircon. Mineral Petrol 39:21–37

Ragland PC, Billings GK, Adams JAS (1967) Chemical fractionation and its relationship to the distribution of thorium and uranium in a zoned granite batholith. Geochim Cosmochim Acta 31(1):17–33

Rudnik RL, Gao S (2003) Composition of the continental crust. In: Rudnick RL, Holland HD, Turekian KK (eds) Treatise on geochemistry, vol 3. Elsevier-Pergamon, Oxford, pp 1–64

Sabet AH (1972) On the stratigraphy of basement rocks of Egypt. Ann Geol Surv Egypt II:79–102

Speer JA (1982) The actinide orthosilicates. In: Ribbe PH (ed) Orthosilicates. Mineral Soc Am, Washington DC, pp 67–113. (Rev Mineral 5)

Sun Q, Chen B, Li Q, Jin H (2024) Distribution and mineralogical features of thorite in the Bayan Obo deposit: implications for hydrothermal metasomatic th re-enrichment. Ore Geol Rev 104:105831

Van Gosen BS, Gillerman VS, Armbrustmacher TJ (2009) Thorium deposits of the United States–Energy resources. for the Future. U.S. Geol Surv Cir 1336

Vasilatos C, Papoutsa A (2023) The REE-Zr-U-Th minerals of the Maronia Monzodiorite, N. Greece: implications on the saturation and segregation mechanisms of critical metals in Intermediate–mafic compositions. Minerals 13(10):1256

von Blanckenburg F (1992) Combined high-precision chronometry and geochemical tracing using accessory minerals: Applied to the Central-Alpine Bergell intrusion (central Europe). Chem Geol 100:19–40

Wedepohl HK (1995) The composition of the continental crust. Geochim Cosmochim Acta 59:1217–1232

Wood SA, Richetts A (2000) Allanite-(Ce) from the Eocene Casto granite, Idaho: response to hydrothermal alteration. Can Mineral 38:81–100

Žáček V, Škoda R, Sulovsky P (2009) U–Th-rich zircon, thorite and allanite-(Ce) as main carriers of radioactivity in the highly radioactive ultrapotassic melasyenite porphyry from the Šumava Mts., Moldanubian Zone. J Geosc (Czech Republ) 54:343–354

Zhang L, Wang F, Zhou T, Chen Z (2023) Contrasting alteration textures and geochemistry of allanite from uranium-fertile and barren granites: insights into granite-related U and ion-adsorption REE mineralization. Am Mineral 108:1298–1314